Rat brains also have a default mode network

Hanbing Lu[a], Qihong Zou[a,b], Hong Gu[a], Marcus E. Raichle[c,1], Elliot A. Stein[a,1], and Yihong Yang[a,1]

[a]Neuroimaging Research Branch, National Institute on Drug Abuse, Intramural Research Programs, National Institutes of Health, Baltimore, MD 21224; [b]MRI Research Center and Beijing City Key Laboratory for Medical Physics and Engineering, Peking University, Beijing 100871, China; and [c]Departments of Radiology, Neurology, Anatomy and Neurobiology, and Biomedical Engineering, Washington University in St. Louis, St. Louis, MO 63110

Contributed by Marcus E. Raichle, January 11, 2012 (sent for review August 16, 2011)

The default mode network (DMN) in humans has been suggested to support a variety of cognitive functions and has been implicated in an array of neuropsychological disorders. However, its function (s) remains poorly understood. We show that rats possess a DMN that is broadly similar to the DMNs of nonhuman primates and humans. Our data suggest that, despite the distinct evolutionary paths between rodent and primate brain, a well-organized, intrinsically coherent DMN appears to be a fundamental feature in the mammalian brain whose primary functions might be to integrate multimodal sensory and affective information to guide behavior in anticipation of changing environmental contingencies.

functional MRI | resting state | intrinsic activity | connectivity | spontaneous fluctuation

In the absence of an immediate need for goal-directed attention to the surrounding environment, our minds wander from recollection of past happenings to imagination of future events. Neuroimaging studies have consistently identified a set of interconnected brain areas that becomes less active during attention-demanding cognitive tasks (1). This so-called default mode network (DMN) is posited to play a fundamental role in brain organization and supports a variety of self-referential functions such as understanding others' mental state, recollection and imagination (2), conceptual processing (3), and even in the sustenance of conscious awareness (4). Many of these functions have been considered to be unique to humans. Intriguingly, similar coherent structures have been shown to exist in anesthetized macaque monkeys and chimpanzees (5, 6). Furthermore, the functions of the default network are disrupted in such neuropsychological disorders as schizophrenia, Alzheimer's disease, and autism (7–9), underscoring the clear and critical need for further investigating the neurobiological basis of DMN using animal models.

The evolutionary clade of rodents is about 35 million years earlier than that of old world monkeys and about 60 million years earlier than humans (10). Although many of the structures and functions of subcortical nuclei are conserved across these three species, the neocortex, in particular the "association" cortex, has extensively expanded in the primate as a result of evolutionary pressure, which is considered to be crucial in the development of higher cognitive and behavioral functions (10, 11). On the other hand, such structures as cingulate cortex, prefrontal cortex, and hippocampal formation, all of which are critical elements of the DMN, are also present in rodents (11). Given the distant evolutionary paths between rodent and primate brain, an intriguing question arises: Does the rat possess a similar DMN? Such a network, once demonstrated, would not only suggest that an operational DMN is a common feature in the mammalian brain, perhaps induced via parallel evolution as a result of natural selection, it would also offer a novel platform to explore the physiological basis and behavioral significance of the DMN. Such a demonstration may also suggest a novel approach for comparing brain development across species.

Results

We probed brain activity using resting state functional magnetic resonance imaging (fMRI), a technique that identifies neuronal networks based on synchronized spontaneous fluctuations (12, 13). Because many anesthetic agents interfere with neural activity and neurovascular coupling, we first developed an anesthesia regime consisting of a combination of dexmedetomidine and isoflurane. In a pilot study (n = 11), the functional status of the rat brain under the above anesthetic regime was assessed by measuring fMRI responses to electrical forepaw stimulation. Each rat was studied on two occasions separated by 1 wk. As shown in Fig. S1, robust fMRI responses were seen 90 min after the experiment was initiated and remained stable during the remaining 3-h experimental period, presumably because anesthesia levels and physiological parameters reached stable, steady-state conditions. Furthermore, the fMRI responses in weeks 1 and 2 were similar, suggesting the appropriateness of this anesthesia regime for longitudinal fMRI study.

After determining the optimum experimental window to maintain stable fMRI responses, we performed a series of resting state fMRI scans on a second group of animals (n = 16) using a single-shot gradient-echo echo-planar imaging (EPI) sequence. A total of 119 scan sessions (260 volumes per session) were acquired by repeated measures separated by 1 wk. Geometrically corrected EPI datasets from individual animals were registered to a common space, followed by slice-timing correction and linear and quadratic trend removal. Group-level independent component analysis (gICA) was applied to identify connectivity patterns. Component maps were overlaid onto a rat digital atlas for structural identification. Consistent with previous reports (14–19), we found multiple networks, including bilateral somatosensory (forepaw and whisker barrel cortex) and insular networks, as shown in Fig. S2.

A particularly interesting network is shown in Fig. 1 (*Left*), which includes the following bilateral structures: ventral, lateral, and rostral medial orbital frontal cortex (OFC, VO, LO, rMO), rostral dorsal prelimbic cortex (PrL), cingulate cortex (Cg1/Cg2), retrosplenial cortex (RSC), granular and dysgranular cortex (RSG/RSD), rostral and dorsal posterior parietal cortex (PtPR, PtPD), and medial secondary visual cortex (V2M). Furthermore, the posterior ventral lateral clusters (area 4 in Fig. 1) include primary/secondary auditory cortex (Au1, AuD, AuV) and the temporal association cortex (TeA). Dorsal hippocampus (CA1) also appears to be involved (but see *Technical Considerations* below). RSG/RSD is the homologous structure of human posterior cingulate cortex (PCC); posterior parietal cortex (PPC) along with V2M belongs to the rat parietal association cortex (20); the orbital areas (VO, LO, rMO), PrL, and anterior cingulate cortex (ACC) are components of the rat prefrontal cortex (11, 21).

Author contributions: H.L., M.E.R., E.A.S., and Y.Y. designed research; H.L. performed research; H.L., Q.Z., H.G., and Y.Y. analyzed data; and H.L., M.E.R., E.A.S., and Y.Y. wrote the paper.

The authors declare no conflict of interest.

Freely available online through the PNAS open access option.

[1]To whom correspondence may be addressed. E-mail: marc@npg.wustl.edu, estein@intra.nida.nih.gov, or yihongyang@intra.nida.nih.gov.

This article contains supporting information online at www.pnas.org/lookup/suppl/doi:10.1073/pnas.1200506109/-/DCSupplemental.

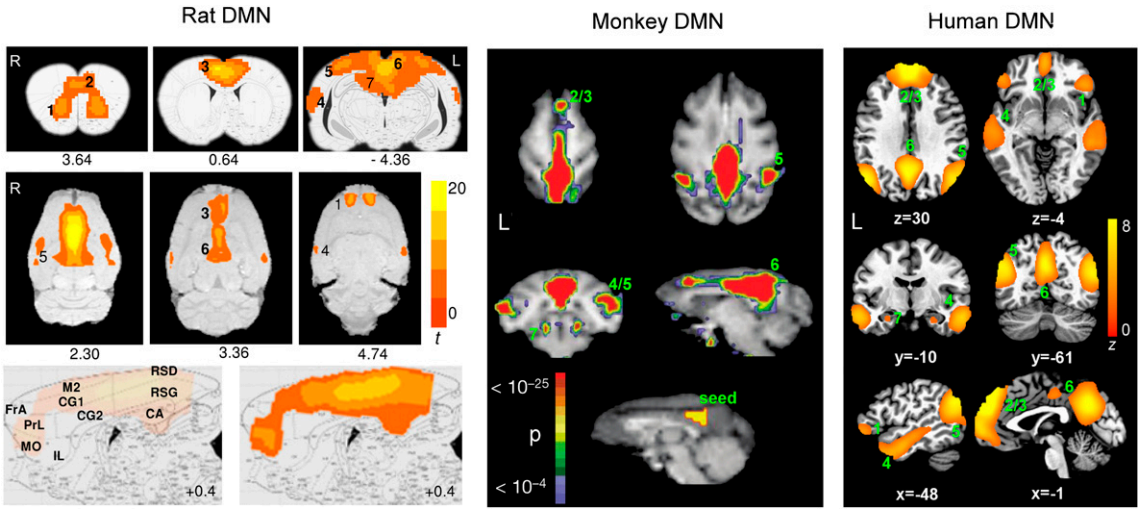

Fig. 1. Comparison of the DMN in rat, monkey, and human. For rat DMN (*Left*), significant clusters include: 1, orbital cortex; 2, prelimbic cortex (PrL); 3, cingulate cortex (CG1, CG2); 4, auditory/temporal association cortex (Au1, AuD, AuV, TeA); 5, posterior parietal cortex; 6, retrosplenial cortex, which corresponds to posterior cingulate cortex in humans; 7, hippocampus (CA1). (*Center*) Connectivity maps in the axial plane. Note the strong connectivity between prefrontal and posterior cingulate cortices, which can best be visualized in the sagittal plane (*Bottom*, medial-lateral: +0.4 mm). FrA, frontal association cortex; MO, medial orbital cortex; R, right; RSG/RSD, granular/dysgranular retrosplenial cortex. Color bar indicates *t* scores ($n = 16$, thresholded at $t > 5.6$, corrected $P < 0.05$). Numbers below images are approximate coordinates relative to bregma. For human DMN (*Right*), significant clusters include: 1, orbital frontal cortex; 2/3, medial prefrontal cortex/anterior cingulate cortex; 4, lateral temporal cortex; 5, inferior parietal lobe; 6, posterior cingulate/retrosplenial cortex; 7, hippocampus/parahippocampal cortex ($n = 39$, thresholded at $z > 2.1$, corrected $P < 0.05$). For monkey DMN (*Center*): 2/3, dorsal medial prefrontal cortex; 4/5, lateral temporoparietal cortex (including area 7a and superior temporal gyrus); 6, posterior cingulate/precuneus cortex; 7, posterior parahippocampal cortex. The monkey DMN map was derived using the cross-correlation method with the seed region shown (*Bottom*) [adapted from Vincent et al. (5)].

The connectivity of this network is broadly similar to the DMN obtained in the human brain using a similar gICA analysis strategy (Fig. 1, *Right*), which includes orbital frontal cortex, medial prefrontal/anterior cingulate cortex, lateral temporal cortex, inferior parietal lobe, posterior cingulate/RSC, and hippocampus/parahippocampal cortex. This network is consistent with that reported in previous findings (2, 13).

The chief difference between the human DMN and the proposed rat DMN is that the connectivity between anterior and posterior cingulate cortices includes the entire medial ridge in the rat brain, which can be best visualized in the sagittal and coronal planes (Fig. 1, *Left*), whereas it remains more focal in the human. Table 1 lists the stereotaxic coordinates and the Brodmann areas (BAs) of individual brain structures involved in the network from rat and human maps, respectively.

Given the distinct evolutionary clades among rodents, old world monkeys, and humans, it would seem beneficial to compare the DMNs across these three species. Shown in Fig. 1 (*Center*) is the DMN in adult macaque monkeys acquired under isoflurane anesthesia (reproduced from ref. 5), which comprises dorsal medial prefrontal cortex, posterior cingulate/precuneus cortex, lateral temporoparietal cortex (including area 7a and superior temporal gyrus), and posterior parahippocampal cortex. The connectivity patterns of monkey DMN share remarkable similarity to the human DMN, suggesting that many elements of the default system are conserved in primates.

Table 1. List of the coordinates of the DMN components in rat and human

Rat DMN				Human DMN			
	Paxino's atlas				Talairach space		
Region	M-L	D-V	A-P	Region	X	Y	Z
Orbital ctx (VO, LO, rMO)	±1.8	5.2	3.64	Orbital frontal ctx (BA 47)	46	31	−1
					−46	37	−3
Prelimbic ctx (CG1/CG2)	±0.6	3.0	3.64	mPFC/ACC (BA 9/10/11/24/32)	1	52	33
	±0.4	2.0	0.64				
Auditory/temporal association ctx	−7.0	5.8	−4.68	Infer temporal gyrus (BA 20/21)	56	−11	−16
	7.4	5.4	−4.68		−55	−5	−18
Post parietal ctx (PtPR, PtPD, V2M)	3.2	1.0	−4.36	Infer parietal ctx (BA 7/39/40)	50	−61	21
	−4.4	1.4	−4.36		−47	−65	29
Retro splenial ctx (RSD/RSG)	±0.4	2.3	−3.36	Post cingulate ctx (BA 23/31)	−2	−58	30
Dorsal hipp	±1.0	4.0	−4.36	Parahipp gyrus/hipp (BA 27/28/35/36)	25	−10	−19
					−25	−11	−18

Coordinates are centers of the mass in individual areas. A-P, D-V, and M-L indicate anterior–posterior, dorsal–ventral, and medial–lateral directions, respectively. A-P and D-V coordinates are based on rat atlas coregistered to MR images. For the M-L coordinates, medial to the left side is defined as negative and to the right side as positive. ctx, cortex; infer parietal ctx, inferior parietal cortex; mPFC, medial prefrontal cortex; parahipp gyrus/hipp, parahippocampal gyrus/hippocampus; PtPR and PtPD, rostral and dorsal posterior parietal cortex (post parietal ctx); V2M, medial secondary visual cortex.

We performed further analyses to characterize the architecture of the proposed default network. Thirteen a priori regions of interest (ROIs) were chosen based on the anatomical structures involved in the network. Graph analysis based on significant functional connections between regions ($P < 5 \times 10^{-4}$, Bonferroni-corrected) showed that RSC and prefrontal cortex acted as hubs of the default network, which exhibited the highest degree of connections with other regions. Network modularity analysis using the simulated annealing algorithm (22) identified two distinct subsystems. Results are shown in Fig. 2. The subsystem that centered on the prefrontal cortex included the cingulate, OFC, and prelimbic cortex, and has strong functional correlation with the temporal cluster (Au1, AuD, AuV, and TeA); the subsystem centered around the RSC has strong functional correlation with hippocampus, PPC, and the secondary visual cortex. Cytoarchitectonically, unlike the granular prefrontal cortex in primates, rat prefrontal cortex is composed exclusively of agranular cortical areas (21). However, despite such differences, the organization shown in Fig. 2 bears remarkable similarity to that of the human DMN (23).

Discussion

Using ICA, a data-driven fMRI data analysis method, we have identified multiple networks in the anesthetized rat brain (e.g., primary somatosensory network) that are homologous to those reported in humans (11). One of those networks, the proposed rodent DMN, is the primary focus of this report. The functional significance of this network and its relationship to the DMN seen in primates (1, 5, 6, 24) remain to be explored. In light of the significant evolutionary divergence of rodents and primates, it may not be surprising that the structural homology across species, although startlingly similar, is not complete. However, neuroanatomical data in the extant literature regarding the structures that constitute the DMN in rodents and primates may be applied to shed light on these questions and are discussed in some detail below.

Neuroanatomical and Functional Considerations. Network analysis (Fig. 2) reveals that one subsystem within the rat DMN includes a frontal cluster. Structures within this cluster belong to the so-called orbital medial prefrontal cortex (OMPFC). Studies in rodents have revealed two networks within OMPFC, namely a "medial network" and an "orbital network" (25, 26), that are broadly similar to those previously discovered in nonhuman primates (27–29). OMPFC projections to such autonomic control structures as periaqueductal gray (PAG) arise exclusively from within the medial, but not the orbital network, as do almost all of the projections to the hypothalamus (25, 26, 30). Such distinctions along with their intrinsic patterns of corticocortical connections and their connections with limbic, sensory, and striatothalamic structures have been taken to define networks within OMPFC (28). Stimulation of the medial network evokes strong autonomic (e.g., blood pressure, heart rate, skin temperature) and endocrine changes along with integrated emotional responses, and has been characterized as an "emotional motor" network. On the other hand, the orbital network receives inputs from multiple sensory modalities, including olfaction, taste, general visceral sensation, somatosensation, and vision, and is characterized as a "viscerosensory" network. In rats, the medial network includes ventral and dorsal ACC, PrL, and infralimbic (IL) cortex on the medial wall, areas MO, VO, and the medial part of ventral lateral orbital (VLO) coretex in the medial edge of the orbital cortex, and areas of dorsal lateral orbital (DLO) and agranular insular (AI) cortex laterally, all of which project to the PAG. The rat orbital network includes ventral AI (AIv), LO, the lateral part of VLO, and parts of the dysgranular (DI) and granular (GI) insular cortex (25).

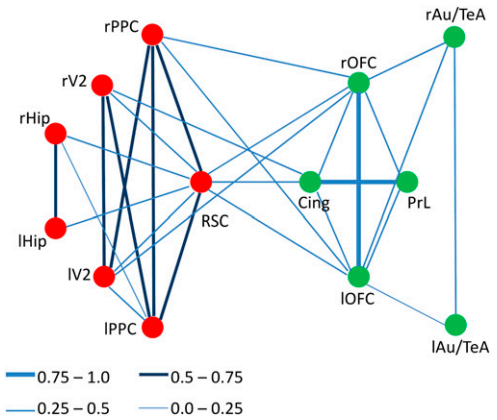

Fig. 2. Functional correlation strengths between 13 brain regions within the DMN show the network separated into two modules: One is a parietal subsystem clustered at RSC, and the other is a temporal-prefrontal subsystem. Lines of different colors and widths represent correlation strength. The thickness of the lines reflects the strength of the correlation between regions. Cing, cingulate cortex (CG1 and CG2); PrL, prelimbic cortex; rAu/TeA and lAu/TeA, right and left auditory/temporal association cortex; rHip and lHip, right and left hippocampus; rOFC and lOFC, right and left orbital frontal cortex; rPPC and lPPC, right and left posterior parietal cortex; RSC, retrosplenial cortex (granular and dysgranular); rV2 and lV2, right and left secondary visual cortex.

As illustrated in Figs. 1 and 2, the proposed rat DMN includes the following medial network structures: ACC, rMO, and a portion of rostral dorsal PrL; VO is also involved. LO is the only orbital network structure that is included within the rat DMN. Notably, it does not include IL, an important region within the medial network, nor does it include the insular orbital network structures [AIv, DI, and GI]. However, insular cortex sends projections to OMPFC, in particular LO, VLO, PrL, and IL (31, 32), and thus, through corticocortical connections (32, 33), highly integrated viscerosensory information reaches the medial and orbital networks of OMPFC.

Projections from other sensory modalities also reach the proposed DMN, and are summarized in Table S1. In addition to the direct involvement of the primary and secondary auditory cortices, the PPC receives extensive projections from the primary and secondary sensory areas (Par1, Par2), secondary occipital areas (OC2M, OC2L), and primary temporal cortex (Au1) (34). Similarly, TeA receives strong inputs from auditory cortex, as well as OC1, OC2M, and OC2L (35). ACC also receives visual (OC1, OC2M) and auditory inputs (35, 36). RSG, besides its strong connections with hippocampus, receives extensive visual inputs (OC2M, OC2L) (34, 37). Thus, it appears that a common feature among the structures involved in the proposed rat DMN is that they are all engaged in integrating high-order information from multiple sensory modalities.

Another feature among the DMN structures is that they receive direct or indirect projections from core limbic structures. Table S1 summarizes major connections from hippocampus/amygdala to the DMN. Previous studies revealed that amygdaloid projections to the PFC predominantly stemmed from the basal amygdaloid nuclei and terminate at both the medial and lateral subdivisions of the PFC (38–40). A retrograde study of rat orbital cortex (31) found that VO, VLO, and LO also receive projections from basomedial and basolateral nuclei of amygdala and perirhinal cortex, and through which indirectly connect with hippocampus (41). RSC is a hub of the DMN (Fig. 2). It is composed of dysgranular (Rdg) and granular cortex (Rga, Rgb); each has extensive connections with the hippocampal formation, which are topographically organized. RSC is connected primarily to the rostrodorsal hippocampal formation, whereas caudal parts of the

RSC are connected with caudoventral areas of the hippocampal formation. The elaborate connections between the RSC and the hippocampal formation suggest that this projection provides an important pathway by which the hippocampus affects learning, memory, and emotional behavior (42).

Thus, it appears clear from the above summary that the structures involved in the proposed rat DMN share two common features: (*i*) They receive high-order information from virtually all sensory modalities, and (*ii*) they have direct or indirect connections with such limbic structures as hippocampus and amygdala, suggesting the involvement of memory and emotional behavior. Based upon observations of patients and laboratory animals with frontal lobe impairment and the neuroanatomical connections of the prefrontal cortex, Nauta posited (43) that the prefrontal cortex receives and processes information about the internal and external milieu of the body by integrating multisensory stimuli (see also refs. 29, 40, and 44), and that the close fronto-limbic relationship enables integration of an organism's somatic sensorimotor and affective responsiveness to act coherently in anticipation of environmental contingencies.

The prefrontal cortex that Nauta considered is a key component of the DMN network shown in Figs. 1 and 2. Given the neuroanatomical characteristics and functional specializations of the DMN structures described above, we propose that the cardinal function of the DMN is to evaluate the internal and external milieu of the body by integrating interoceptive and exteroceptive information from multiple modalities. In doing so, the brain functions as a "Bayesian machine" (45), making inference and guiding action in a timely and environmentally relevant fashion.

The proposed rodent DMN could have evolutionary significance. To avoid attack from predators for survival, this "intelligence oversight" system must remain alert, demanding default, nonstop coherent activity. This might help explain why this system requires high basal cerebral blood flow and metabolism, a hallmark that has long been recognized (1). Because key components within the network, such as orbital and medial PFC, ACC, and RSC, are also involved in higher cognitive functions, it may also explain why cognitive tasks tapping into this system induce a negative fMRI response within the DMN, because these tasks interrupt ongoing network activity. Impaired information transfer between frontal-parietal association cortices was reported during inhalational anesthesia, suggesting a role of frontal-parietal interactions in consciousness (46, 47). This might, at least in part, underlie the neural mechanism of the DMN in sustaining conscious awareness in humans (4). The existence of the DMN under general anesthesia in both nonhuman primates (5) and now in rodents suggests that the basic function of the DMN may not be limited to self-referential behavior as suggested by studies in conscious human subjects, because such behavior is presumably supported by consciousness.

Comparison of Rat, Monkey, and Human DMN. Although the DMNs across rat, monkey, and human are broadly similar (Fig. 1), the differential involvement of OMPFC structures across these three species is particularly puzzling. As summarized in Table 1, human DMN involves BA 9, 10, 11, 24, 32, and 47. The medial wall areas BA 10, 11, 24, and 32 and dorsomedial prefrontal cortex (BA 9) likely belong to the medial network of OMPFC. Human BA 47 appears to correspond to area 12 in monkey (21), and likely belongs to the OMPFC network. Thus, human DMN comprises extensive medial network structures with the exception of area 47, which belongs to the orbital network.

In contrast, medial wall structures IL and a large part of PrL are not involved in the proposed rat DMN. Only LO, an orbital network structure, along with medial network structure VO and rostral MO and ACC, appear to be constituents of the DMN. Furthermore, rat DMN includes the entire cingulate cortex (ACC and RSD/RSG), whereas only portions of ACC (BA 24 and 32) and PCC (BA 23 and 31) are constituents of human DMN. Interestingly, monkey DMN comprises only a few frontal structures, namely the dorsal medial prefrontal cortex, but it includes extensive posterior cingulate/precuneus cortex. These differences might reflect either species-specific functional differences or may be attributable to behavioral state, because both the monkeys and rats were scanned under anesthesia and presumably in a different consciousness state from the awake humans (*Technical Considerations*). Future work may reveal the potential neurobiological significance of the differential engagement of OMPFC and cingulate cortex across species.

The DMNs across the three species comprise extensive lateral temporoparietal cortex. However, whereas the inferior parietal cluster of the human DMN includes BA 39 and 40, neither appears to have a clear homolog in monkeys (48, 49), nor probably more so in rats. Furthermore, the temporal cluster of the rat DMN includes primary and secondary auditory cortex, which are not directly seen in the human DMN. Instead, the human DMN includes BA 20 and 21, the association cortices involved in auditory and language processing, high-level visual processing, and recognition. Once again, such distinctions might reflect species-specific evolution of the DMN.

Relationship Between Structural and Functional Connectivity. In general, direct anatomical connections have been reported between the structures implicated in the DMN, as summarized in Table S2. In this regard, the study by Reep et al. (34) is particularly informative, wherein the topography of corticocortical and thalamic connections of rat PPC was systematically investigated using classical tracing techniques. Injection of retrograde tracers into PPC and retrosplenial cortex led to dense labeling in OFC, ACC, OC2, secondary parietal cortex (par 2), and temporal association cortex. Notably, the corticocortical connection pattern shown in figure 4 of ref. 34 bears remarkable similarity to the functional connectivity pattern of Fig. 1 in this study, suggesting that functional connectivity as measured by fMRI is indeed constrained by anatomical connections, as previously suggested (50, 51). On the other hand, interconnections between structures do not guarantee a functional network. For example, the mediodorsal thalamic nuclei are known to be connected with the rat OMPFC (38); however, it is not seen in the rat DMN. Thus, our data support the notion that functional connectivity is constrained by anatomical connections, and that the proposed default network is organized by function instead of simple anatomical connections (5, 50, 51).

Technical Considerations. Several technical issues need to be considered when interpreting our data. First, the present study was performed under anesthesia. Anesthetic agents influence brain functions, and such effects are likely to be species-specific. In the present study, we used dexmedetomidine (an active enantiomer of medetomidine) in combination with a low dose of isoflurane. Dexmedetomidine, an α_2-agonist routinely used in human medical practice, produces dose-dependent sedative effects along with analgesia, muscle relaxation, and anxiolysis. It was recently introduced for longitudinal functional MRI and resting state fMRI studies in rodents (15, 52). However, the sedative effect of medetomidine is reduced with constant infusion of medetomidine alone, and a stepwise dose increase has been suggested to maintain stable sedation (17). In pilot studies, we used a combination of low-dose isoflurane (0.25%) and dexmedetomidine (0.03 mg/kg i.v.), and were able to maintain stable sedation for over 4 h with successful repeated fMRI experiments on the same animal (Fig. S1). Under the anesthesia regime that we developed, we found differential engagement of the orbital and medial networks in rat and human DMN, as discussed above. Even though it is tantalizing to think that such differences might reveal

DMNs that are species-specific, we cannot rule out the possibility that they were biased by anesthesia.

Second, the nominal imaging resolution in this study is 547 × 547 μm^2 with a slice thickness of 1 mm. Such a relatively coarse resolution limits our ability to differentiate the boundaries between small yet distinct structures that are spatially close, for example, medial network structure VO from orbital network structure LO. For the same reason, we cannot rule out the possibility that the statistical map covering dorsal hippocampus (area 7 in the rat DMN; Fig. 1) may have resulted from a partial volume effect from neighboring RSD/RSG. Future high-resolution studies may help clarify this uncertainty. Third, due to strong magnetic field inhomogeneity that exists in the interface between ear canal and brain tissue, our imaging coverage of the caudal ventrolateral structures, in particular the amygdala, was very poor. This also affected, although to a lesser degree, the signal from the temporal areas, including perirhinal and entorhinal cortices, which may have compromised the detection of some of the temporal areas that could potentially be involved in the DMN.

Despite the above technical limitations, this study reveals that rats possess a coherent, intrinsic network that is broadly similar to the monkey and human DMNs. Neuroanatomical and functional connectivity of the proposed default network suggests that, although its role in cognitive function and behavior has clearly differentially evolved across species, a well-organized, coherent intrinsic default brain network may be a fundamental feature in the mammalian brain. We propose that the primary function of the rat DMN might be to evaluate internal and external body states by assessing information from multiple sensory modalities and, by integrating with past experience, to anticipate changing environmental contingencies.

Materials and Methods

Animal Preparation for MRI. Anesthesia was induced with 3% isoflurane followed by intramuscular administration of the α_2-agonist (dexmedetomidine; 0.015 mg/kg). During initial scanning, isoflurane (1%) in oxygen-enriched air was delivered via a customized nose cone with continuous intramuscular infusion of dexmedetomidine (0.03 $mg \cdot kg^{-1} \cdot hr^{-1}$). Core body temperature, arterial oxygen saturation level, and cardiac and respiration rates were maintained within normal ranges. After the anatomical localization scans were acquired, isoflurane concentration was reduced to 0.25%. The typical respiration rate ranged from 45 bpm when the scan started and gradually increased to 70–85 bpm. In some cases, when the respiration rate increased to 90 bpm, isoflurane was adjusted to 0.5%.

Resting State fMRI in Rats. Animal MRI experiments were performed on a Bruker Biospin 9.4T scanner. To assess the functional status of the brain under the above anesthetic regime, we performed a pilot experiment on a separate group of animals (n = 11) by measuring the fMRI responses to electrical forepaw stimulation. The stimulation paradigm consisted of three alternating cycles of 30 s ON/30 s OFF, starting with a 20-s baseline. This was repeated every 15 min for about 4.5 h. Each rat in the pilot group was studied on two occasions separated by 1 wk.

After determining that the optimum experimental window for stable evoked blood oxygenation level-dependent (BOLD) responses began about 90 min after the initiation of dexmedetomidine infusion (Fig. S1), we performed a series of resting state fMRI scans on a second group of animals (n = 16) using a single-shot gradient-echo EPI (GE-EPI) sequence. Scan parameters were: field of view = 3.5 cm, matrix size = 64 × 64, echo time = 15 ms, and repetition time = 1,000 ms, 11 slices with a thickness of 1 mm. A total of 260 volumes of images was collected during each session, with a total of 119 scan sessions from the 16 animals. All imaging procedures were approved by the National Institute on Drug Abuse (NIDA) Animal Care and Use Committee.

Data Analysis. ***Identification of rat DMN.*** Geometric distortions in EPI images were corrected using the PLACE method (53). Data preprocessing included slice-timing correction, linear and quadratic trend removal, and spatial smoothing with a Gaussian kernel (full width at half maximum = 0.6 mm). Images from individual animals were then coregistered onto a common 3D space aligned with a rat stereotaxic atlas using an approach previously described (54, 55). Analyses were performed within the AFNI framework (56).

Resting state fMRI data were analyzed using gICA within the FSL software package (57). The number of components was set to 30. To evaluate the robustness of the component maps identified by ICA, we performed follow-up analyses by setting the number of components to 20 and 40 (Fig. S3). Between-subject analysis and group statistical comparison were conducted using the dual-regression approach (58). Component maps were coregistered to a high-resolution rat digital atlas to aid in structural identification (55).

Network analysis of rat DMN. Thirteen a priori ROIs were chosen based on the anatomical structures comprising the network. Pearson correlation coefficients of the average time courses between each ROI pair were computed and subjected to one-sample t tests against zero after z transformation. A Bonferroni-corrected significance level of $P < 0.0005$ was used to threshold the correlation matrix into a binarized matrix whose element is 1 if there is significant correlation between two brain regions and 0 otherwise. The degree of each ROI was calculated and the ROIs with the highest degree were considered as network hubs.

The modularity of the network was analyzed based on the method described by Newman and Girvan (59). The modularity index quantifies the difference between the number of intramodule links of the actual network and that of a random network in which connections are linked at random. The aim of this module identification process is to find a specific partition that yields the largest network modularity. Nonlinear optimization using the simulated annealing approach was used to find the partition (22).

Human resting state fMRI data acquisition and analysis. Whole-brain resting state fMRI data were acquired with a Siemens Allegra 3T scanner using a standard single-shot GE-EPI sequence (n = 39). Data preprocessing was the same as described above. Preprocessed data were transformed to the standard Talairach space. An unbiased group-wise nonlinear registration method based upon a small deformation elastic model (60) was applied to further align the resting state functional data across subjects. Each subject's dataset was then concatenated temporally. Group ICA (57) was used to generate 20 component maps. The study protocol was approved by the Institutional Review Board of the NIDA Intramural Research Program. Complete methodological details are described in *SI Materials and Methods*.

ACKNOWLEDGMENTS. We acknowledge the invaluable assistance of Joseph L. Price, Professor of Anatomy and Neurobiology, Washington University School of Medicine, who gave generously of his time in helping us interpret our imaging findings in the context of rat brain anatomy. This study is supported by the Intramural Research Program of the National Institute on Drug Abuse, National Institutes of Health. M.E.R. is supported by Grant NS06833 from the National Institute of Neurological Disorders and Stroke. Q.Z. is supported by China's National Strategic Basic Research Program ("973") Grant 2012CB720700.

1. Raichle ME, et al. (2001) A default mode of brain function. *Proc Natl Acad Sci USA* 98: 676–682.
2. Buckner RL, Andrews-Hanna JR, Schacter DL (2008) The brain's default network: Anatomy, function, and relevance to disease. *Ann N Y Acad Sci* 1124:1–38.
3. Binder JR, et al. (1999) Conceptual processing during the conscious resting state. A functional MRI study. *J Cogn Neurosci* 11:80–95.
4. Horovitz SG, et al. (2009) Decoupling of the brain's default mode network during deep sleep. *Proc Natl Acad Sci USA* 106:11376–11381.
5. Vincent JL, et al. (2007) Intrinsic functional architecture in the anaesthetized monkey brain. *Nature* 447:83–86.
6. Rilling JK, et al. (2007) A comparison of resting-state brain activity in humans and chimpanzees. *Proc Natl Acad Sci USA* 104:17146–17151.
7. Bluhm RL, et al. (2007) Spontaneous low-frequency fluctuations in the BOLD signal in schizophrenic patients: Anomalies in the default network. *Schizophr Bull* 33: 1004–1012.
8. Greicius MD, Srivastava G, Reiss AL, Menon V (2004) Default-mode network activity distinguishes Alzheimer's disease from healthy aging: Evidence from functional MRI. *Proc Natl Acad Sci USA* 101:4637–4642.
9. Kennedy DP, Courchesne E (2008) The intrinsic functional organization of the brain is altered in autism. *Neuroimage* 39:1877–1885.
10. Kaas JH (2005) From mice to men: The evolution of the large, complex human brain. *J Biosci* 30:155–165.
11. Kolb B (1990) Association cortex in the rat. *The Cerebral Cortex of the Rat*, eds Kolb B, Tees RC (MIT Press, Cambridge, MA), pp 433–435.
12. Biswal B, Yetkin FZ, Haughton VM, Hyde JS (1995) Functional connectivity in the motor cortex of resting human brain using echo-planar MRI. *Magn Reson Med* 34: 537–541.
13. Greicius MD, Krasnow B, Reiss AL, Menon V (2003) Functional connectivity in the resting brain: A network analysis of the default mode hypothesis. *Proc Natl Acad Sci USA* 100:253–258.

14. Lu H, et al. (2007) Synchronized delta oscillations correlate with the resting-state functional MRI signal. *Proc Natl Acad Sci USA* 104:18265–18269.
15. Zhao F, Zhao T, Zhou L, Wu Q, Hu X (2008) BOLD study of stimulation-induced neural activity and resting-state connectivity in medetomidine-sedated rat. *Neuroimage* 39: 248–260.
16. Hutchison RM, Mirsattari SM, Jones CK, Gati JS, Leung LS (2010) Functional networks in the anesthetized rat brain revealed by independent component analysis of resting-state FMRI. *J Neurophysiol* 103:3398–3406.
17. Pawela CP, et al. (2009) A protocol for use of medetomidine anesthesia in rats for extended studies using task-induced BOLD contrast and resting-state functional connectivity. *Neuroimage* 46:1137–1147.
18. Liang Z, King J, Zhang N (2011) Uncovering intrinsic connectional architecture of functional networks in awake rat brain. *J Neurosci* 31:3776–3783.
19. Majeed W, et al. (2011) Spatiotemporal dynamics of low frequency BOLD fluctuations in rats and humans. *Neuroimage* 54:1140–1150.
20. Torrealba F, Valdés JL (2008) The parietal association cortex of the rat. *Biol Res* 41: 369–377.
21. Price JL (2007) Definition of the orbital cortex in relation to specific connections with limbic and visceral structures and other cortical regions. *Ann N Y Acad Sci* 1121:54–71.
22. Guimerà R, Sales-Pardo M, Amaral LA (2004) Modularity from fluctuations in random graphs and complex networks. *Phys Rev E Stat Nonlin Soft Matter Phys* 70:025101.
23. Andrews-Hanna JR, Reidler JS, Sepulcre J, Poulin R, Buckner RL (2010) Functional-anatomic fractionation of the brain's default network. *Neuron* 65:550–562.
24. Mantini D, et al. (2011) Default mode of brain function in monkeys. *J Neurosci* 31: 12954–12962.
25. Floyd NS, Price JL, Ferry AT, Keay KA, Bandler R (2000) Orbitomedial prefrontal cortical projections to distinct longitudinal columns of the periaqueductal gray in the rat. *J Comp Neurol* 422:556–578.
26. Floyd NS, Price JL, Ferry AT, Keay KA, Bandler R (2001) Orbitomedial prefrontal cortical projections to hypothalamus in the rat. *J Comp Neurol* 432:307–328.
27. An X, Bandler R, Ongür D, Price JL (1998) Prefrontal cortical projections to longitudinal columns in the midbrain periaqueductal gray in macaque monkeys. *J Comp Neurol* 401:455–479.
28. Ongür D, An X, Price JL (1998) Prefrontal cortical projections to the hypothalamus in macaque monkeys. *J Comp Neurol* 401:480–505.
29. Ongür D, Price JL (2000) The organization of networks within the orbital and medial prefrontal cortex of rats, monkeys and humans. *Cereb Cortex* 10:206–219.
30. Carmichael ST, Price JL (1996) Connectional networks within the orbital and medial prefrontal cortex of macaque monkeys. *J Comp Neurol* 371:179–207.
31. Reep RL, Corwin JV, King V (1996) Neuronal connections of orbital cortex in rats: Topography of cortical and thalamic afferents. *Exp Brain Res* 111:215–232.
32. Gabbott PL, Warner TA, Jays PR, Bacon SJ (2003) Areal and synaptic interconnectivity of prelimbic (area 32), infralimbic (area 25) and insular cortices in the rat. *Brain Res* 993:59–71.
33. Allen GV, Saper CB, Hurley KM, Cechetto DF (1991) Organization of visceral and limbic connections in the insular cortex of the rat. *J Comp Neurol* 311:1–16.
34. Reep RL, Chandler HC, King V, Corwin JV (1994) Rat posterior parietal cortex: Topography of corticocortical and thalamic connections. *Exp Brain Res* 100:67–84.
35. Vaudano E, Legg CR, Glickstein M (1991) Afferent and efferent connections of temporal association cortex in the rat: A horseradish peroxidase study. *Eur J Neurosci* 3: 317–330.
36. Condé F, Maire-Lepoivre E, Audinat E, Crépel F (1995) Afferent connections of the medial frontal cortex of the rat. II. Cortical and subcortical afferents. *J Comp Neurol* 352:567–593.
37. Vogt BA, Miller MW (1983) Cortical connections between rat cingulate cortex and visual, motor, and postsubicular cortices. *J Comp Neurol* 216:192–210.
38. Krettek JE, Price JL (1977) Projections from the amygdaloid complex to the cerebral cortex and thalamus in the rat and cat. *J Comp Neurol* 172:687–722.
39. McDonald AJ (1991) Organization of amygdaloid projections to the prefrontal cortex and associated striatum in the rat. *Neuroscience* 44:1–14.
40. Groenewegen HJ, Uylings HB (2000) The prefrontal cortex and the integration of sensory, limbic and autonomic information. *Prog Brain Res* 126:3–28.
41. Deacon TW, Eichenbaum H, Rosenberg P, Eckmann KW (1983) Afferent connections of the perirhinal cortex in the rat. *J Comp Neurol* 220:168–190.
42. van Groen T, Wyss JM (1992) Connections of the retrosplenial dysgranular cortex in the rat. *J Comp Neurol* 315:200–216.
43. Nauta WJ (1971) The problem of the frontal lobe: A reinterpretation. *J Psychiatr Res* 8:167–187.
44. Van Eden CG, Buijs RM (2000) Functional neuroanatomy of the prefrontal cortex: Autonomic interactions. *Prog Brain Res* 126:49–62.
45. Knill DC, Pouget A (2004) The Bayesian brain: The role of uncertainty in neural coding and computation. *Trends Neurosci* 27:712–719.
46. Imas OA, Ropella KM, Ward BD, Wood JD, Hudetz AG (2005) Volatile anesthetics disrupt frontal-posterior recurrent information transfer at gamma frequencies in rat. *Neurosci Lett* 387:145–150.
47. Alkire MT, Hudetz AG, Tononi G (2008) Consciousness and anesthesia. *Science* 322: 876–880.
48. Karnath HO (2001) New insights into the functions of the superior temporal cortex. *Nat Rev Neurosci* 2:568–576.
49. Roland P (1980) The posterior parietal association cortex in man. *Behav Brain Sci* 3: 513–514.
50. Johnston JM, et al. (2008) Loss of resting interhemispheric functional connectivity after complete section of the corpus callosum. *J Neurosci* 28:6453–6458.
51. Krienen FM, Buckner RL (2009) Segregated fronto-cerebellar circuits revealed by intrinsic functional connectivity. *Cereb Cortex* 19:2485–2497.
52. Weber R, Ramos-Cabrer P, Wiedermann D, van Camp N, Hoehn M (2006) A fully noninvasive and robust experimental protocol for longitudinal fMRI studies in the rat. *Neuroimage* 29:1303–1310.
53. Xiang QS, Ye FQ (2007) Correction for geometric distortion and N/2 ghosting in EPI by phase labeling for additional coordinate encoding (PLACE). *Magn Reson Med* 57: 731–741.
54. Lu H, et al. (2007) Cocaine-induced brain activation detected by dynamic manganese-enhanced magnetic resonance imaging (MEMRI). *Proc Natl Acad Sci USA* 104: 2489–2494.
55. Lu H, et al. (2010) Registering and analyzing rat fMRI data in the stereotaxic framework by exploiting intrinsic anatomical features. *Magn Reson Imaging* 28:146–152.
56. Cox RW (1996) AFNI: Software for analysis and visualization of functional magnetic resonance neuroimages. *Comput Biomed Res* 29:162–173.
57. Beckmann CF, DeLuca M, Devlin JT, Smith SM (2005) Investigations into resting-state connectivity using independent component analysis. *Philos Trans R Soc Lond B Biol Sci* 360:1001–1013.
58. Filippini N, et al. (2009) Distinct patterns of brain activity in young carriers of the APOE-epsilon4 allele. *Proc Natl Acad Sci USA* 104:7209–7214.
59. Newman ME, Girvan M (2004) Finding and evaluating community structure in networks. *Phys Rev E Stat Nonlin Soft Matter Phys* 69:026113.
60. Geng X, Christensen GE, Gu H, Ross TJ, Yang Y (2009) Implicit reference-based group-wise image registration and its application to structural and functional MRI. *Neuroimage* 47:1341–1351.